

Ultrastable Combined Planar-Fiber Plasmon Sensor

Kirill A. Tomyshev,* Diana K. Tazhetdinova, Egor S. Manuilovich, and Oleg V. Butov

A new design for a hybrid fiber-planar refractive index sensor based on the surface plasmon resonance effect is presented. The key element of the design is a thin layer of gold covering a tilted fiber Bragg grating. In the study, a specially developed microfluidic chip is used to perform measurements directly in the flow of the investigated liquid. Rigidly mounting the sensor to the base of the fluid chip is proposed. The presented experimental data demonstrate the high stability of the sensor readings and the low noise level during measurements in a liquid flow. The proposed construction is a promising decision for application in compact immunoassay systems based on microfluidic technologies.

based on a tilted fiber Bragg grating (TFBG),^[8,12–17] which effectively excites a discrete set of cladding modes that interact with the cylindrical surface of the fiber.^[18] Such a sensor has potentially high measurement accuracy.

However, in practice, it is difficult to provide the stability of the fiber sensor's readings. The main reasons for this are the instability of the light polarization and the possible mechanical and acoustic impacts on the sensor during the measurement. The first problem was solved by using a polarization maintaining fiber,^[19,20] but the second has remained unresolved until now. For example, in practice, the sensor can be used in a low flow of liquid, such as in microfluidic cells for immunoassay,^[16,21]

1. Introduction

Plasmon sensors are an actual trend in modern sensorics and are already actively used in immunoassay systems.^[1,2] The operating principle of such sensors is based on the excitation of surface plasmon-polaritons on a thin metal layer by means of optical radiation.^[3–5] In this case, the effective energy transfer of optical radiation occurs when the projection of the phase velocity of the incident light coincides with the propagation velocity of the surface plasmon, which is called surface plasmon resonance (SPR) generation. In turn, the propagation velocity of the plasmon directly depends on the refractive index of the dielectric medium.^[3,4] When the refractive index changes, the plasmon propagation velocity also changes. This principle of work underlies the most common planar measuring complexes, which are based on the well-known Otto and Kretschmann schemes.^[6,7] However, such systems are expensive, complex, and have low mobility.

Sensors based on optical fibers can be a promising alternative to planar sensor design.^[4,8–11] Among the obvious advantages of fiber sensors are their compactness, mobility, and cheapness. The excitation of surface plasmons in optical fibers occurs due to the interaction of propagating optical modes' radiation, with the external surface of a sensor being coated with a thin metal layer. One of the promising designs of the plasmon fiber sensor is

which leads to fluctuations in the fiber and the appearance of strong signal deviations. The simple two-point mounting of the sensor makes it resemble a stretched string that is sensitive to both the fluid flow velocity and to the external acoustic and mechanical stress. Single-point mounting of the sensor probe does not provide a rigid attachment, which further leads to deformations of the sensor in the flow and a disruption in the stability of its readings. In this paper, we propose a possible solution to the problem, which allows us to combine the advantages of stable planar sensors and fiber technologies.

2. Experimental Section


2.1. Sample Production

The fiber part of the sensor design is based on a well-known technology for generating plasmon resonance in optical fibers with the help of a TFBG.^[8,12–17] The grating inscription was produced by the emission of an ArF excimer laser on a wavelength of 193 nm using a phase mask. To create the tilt angle, the plane of the mask, in addition to the fiber, was rotated at an angle to the plane of the front of the laser radiation.^[13] The grating was inscribed in a standard Corning SMF-28 telecommunication fiber. To improve the inscription efficiency, the fiber was loaded with hydrogen at a pressure of 130 bar and a temperature of 70 °C for 48 h. The tilt angle was 11°. In the next stage, the surface of the optical fiber with the grating was covered with a layer of gold that was 40 nm thick using the thermal evaporation of a metal under vacuum conditions. The fiber was rotated along its axis during the evaporation process to provide uniform thickness of the golden layer.^[12]

A microfluidic chip was fabricated with which to conduct experiments in the flow of the investigated liquid. The chip consists of two parts: a flat base made of polymethylmethacrylate

K. A. Tomyshev, D. K. Tazhetdinova, Dr. O. V. Butov
Kotel'nikov Institute of Radioengineering and Electronics of RAS
Mokhovaya 11-7, Moscow 125009, Russia
E-mail: atom@mail.mipt.ru; scatterdice@gmail.com

Dr. E. S. Manuilovich
N. M. Emanuel' Institute of Biochemical Physics of RAS
Kosigyna 4, Moscow 119334, Russia

 The ORCID identification number(s) for the author(s) of this article can be found under <https://doi.org/10.1002/pssa.201800541>.

DOI: 10.1002/pssa.201800541

and a polymethylmethacrylate cover, in which the structure of microfluidic channels is created. There are also two ports for the entry and exit of the liquid on the outer surface of the cover. After incorporating the fiber element into the chip structure, its two parts are glued together and sealed (**Figure 1**). Such a chip is a prototype of a real microfluidic chip, which can be used in immunoassay systems. To carry out the measurements, the investigated liquid is pumped through the chip and interacts with the sensor installed inside.

The key feature of the proposed design of the sensor element is the rigid adhesive bonding of the fiber sensor with the base of the microfluidic chip along the entire length. Obviously, inscribing a TFBG breaks the cylindrical symmetry of the system, thereby making the sensor a plane-symmetrical element. During the inscription of the grating, we made special marks to help us orient the fiber toward the tilt angle. After the deposition of the golden layer, this allowed us to glue the fiber sensing element into the base of the microfluidic chip and orient the plane of the tilt relative to the plane of the base, as shown in **Figure 1**. To conveniently install the sensor onto the base, a narrow groove with a depth of about 30 μm was created to better position of the optical fiber. The sensor was glued to the groove along the entire length.

Obviously, even in case the correct orientation of the Bragg grating plane was chosen during the sensor installation onto the chip, the glue connection can also affect the sensor readings. To minimize this influence, an adhesive was selected with a refractive index, the value of which significantly exceeds the refractive index of the liquids under investigation.

To conduct a comparative experiment, we made a similar chip, in the channel of which a similar fiber sensor was installed, but only with two points of mounting: at the beginning and at the end of the microfluidic channel. The sensor was suspended and completely washed by letting a fluid flow through the microfluidic channel.

2.2. Experimental Setup

The experimental setup to measure the refractive index in a liquid flow using a microfluidic chip is shown in **Figure 2**. The

sensor element (5) mounted on a microfluidic chip (4) was connected via a fiber interface to the multichannel Bragg interrogator Micron Optics SM125-500 with a full spectral range of 1510–1590 nm, and two parallel channels of the interrogator were used simultaneously. Because the interrogation goes to all channels of the interrogator at the same time, one of the two channels can be used as a source and the other as a signal receiver to measure the transmission spectrum. For this purpose, an optical isolator (2) was installed into the circuit, blocking the intrinsic radiation of the receiving channel.

Only one of the two orthogonal linear components of polarization is suitable for surface plasmon resonance excitation. Therefore, to obtain the most contrasting spectral pattern of plasmon resonance, a mechanical polarization controller was installed directly in front of the microfluidic chip from the source side to adjust the sensor before the experiment.

The microfluidic chip was connected to a syringe pump (6) driven by a stepping motor, allowing the volume and velocity of the liquid being pumped through a microfluidic chip to be precisely dosed. The liquid was taken from the tank (7). For the experiment, distilled water and solutions of isopropyl alcohol of various concentrations were used as the test liquids. The refractive index of the liquid was calculated from the concentration of the solution.

2.3. Spectrum Processing

The transmission spectrum of a fiber plasmon sensor based on a TFBG is shown in **Figure 3**. The spectrum was normalized by removing low frequencies in a Fourier transform. The sequence of spectral extrema reflects a discrete set of excited cladding modes. The energy of fiber modes matching the plasmon resonance condition is effectively transferred to the surface plasmon's energy, which is reflected in the form of a characteristic constriction in the transmission spectrum of the sensor. The spectral position of the constriction depends on the refractive index of the surrounding medium.

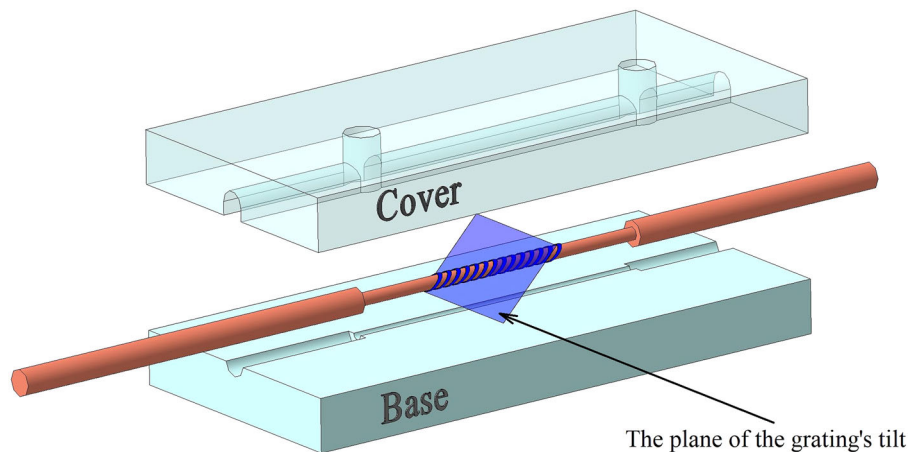


Figure 1. Sensor installation scheme.

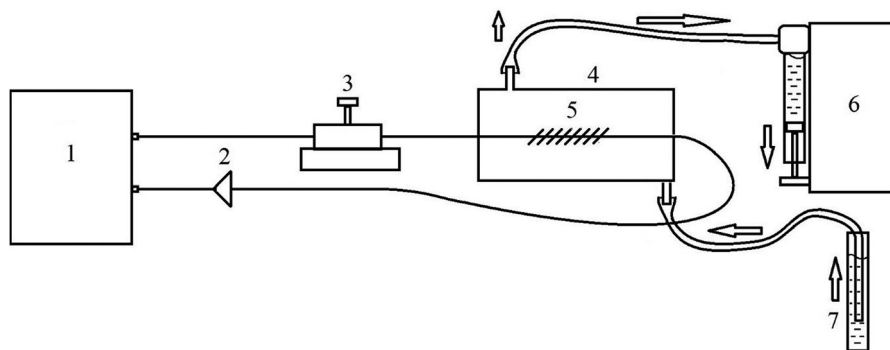


Figure 2. Experimental setup. 1 – interrogator; 2 – fiber isolator; 3 – mechanical polarization controller; 4 – flow cell; 5 – sensing element; 6 – syringe pump; 7 – container with the investigated liquid.

To obtain high measurement accuracy, it is necessary to provide an accurate determination of the plasmon resonance wavelength and its variation with small changes in the refractive index. In a number of publications, observing the spectral position of plasmon resonance by measuring the intensity of one of the spectral peaks close to the spectral constriction is proposed.^[16,22–24] However, in real conditions, such an analysis gives a high probability of error, low reproducibility, and the inability to perform measurements across a wide range of refractive indices. In our work, we use a wide spectral region for a complex analysis of changes in the transmission spectrum of the sensor. The analysis is based on the calculation of the function extremum constructed over all spectral peaks near the spectral constriction. In this case, each peak undergoes an approximation step for a more accurate calculation of its intensity and spectral position.

The mathematical zero of the resulting curve derivative determined the calculated wavelength of the plasmon resonance. In detection tasks, it is important to determine the magnitude of the plasmon resonance wavelength variation under changing external conditions, but not the exact spectral position of the resonance.

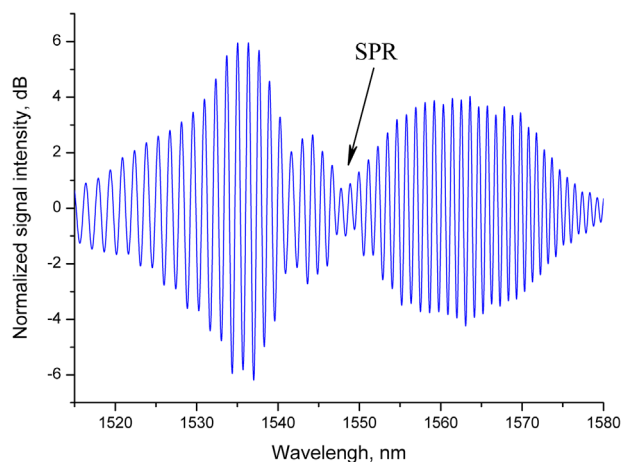


Figure 3. Normalized spectrum of a plasmon sensor based on a tilted fiber Bragg grating incorporated to the planar construction.

3. Results and Discussions

Using the setup shown in Figure 2, we performed a series of experiments with aqueous solutions of isopropyl alcohol of various concentrations from distilled water to a concentration of 1:20. The flow rate of the liquid was estimated based on the speed of the pump and the diameter of the channel and was 50 mm s^{-1} . The measurements were carried out every 10 s during the entire experiment. **Figure 4** shows the results of small concentrations' measurements in the form of the dependence of the plasmon resonance wavelength change on time after the automatic processing of the spectra. The growth of the wavelength corresponds to the growth of the refractive index of the measured solution. Steps on the graph correspond to changes in the concentration of the solution entering the chip. The graph shows the high temporal stability of the readings and the reproducibility of the measurement results using water that was fed into the chip at the beginning and at the end of the experiment as an example. Some drifts of the baselines could be observed, that are related to air bubbles trapping in the channel due to the construction imperfection. These drifts are not caused by the sensor, so the drift regions are not considered when making measurements.

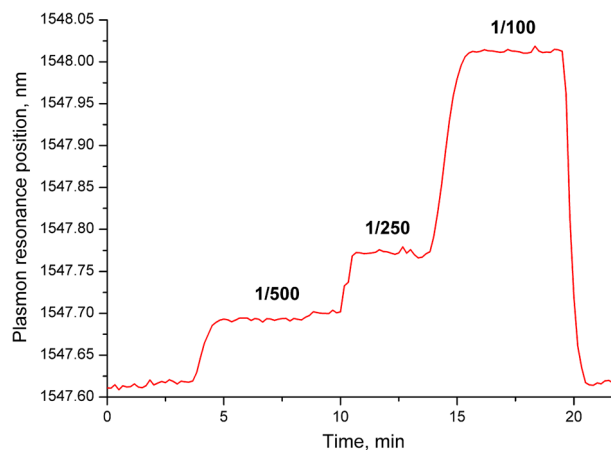


Figure 4. Surface plasmon resonance wavelength position over time.

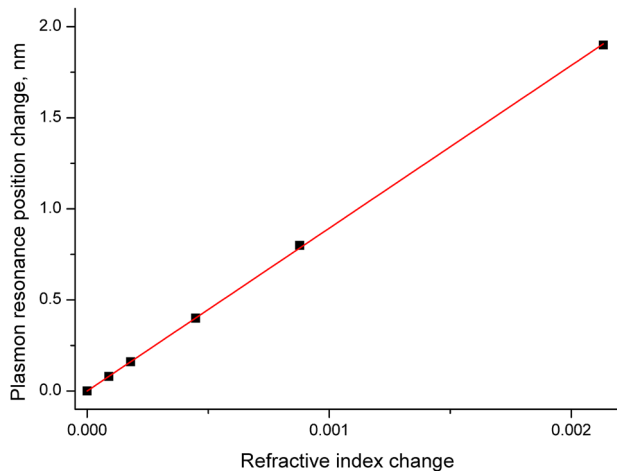


Figure 5. Experimental dependence of the plasmon resonance wavelength change on the solution's refractive index change.

The experimental dependence of the plasmon resonance wavelength change on the magnitude of the refractive index change was constructed based on the measurements. The experimental data were approximated by a straight line (Figure 5). From the slope of the line, according to the known refractive indices of isopropanol solutions,^[25] we can estimate the sensitivity of the sensor to the refractive index unit (RIU), which amounted to 894 nm RIU^{-1} .

As noted above, the principal design solution for using the sensor in a microfluidic chip was to rigidly mount the sensor to the base of the chip along its entire length (planar-fiber sensor), which should significantly improve the stability and reproducibility of the readings. We performed comparative measurements using a sample chip, where the sensor was mounted only at two points. The measurements were carried out under the same conditions, using distilled water for 6 min with a measurement step of 10 s. The measurement data are shown in Figure 6. The solid line shows the scatter of the sensor readings while fixed along the entire length; the dashed line demonstrates the experimental data for the sensor fixed at two points. The graph in Figure 6 shows that the scatter in the planar-fiber sensor is about three times less than that of the classic fiber. This result was obtained due to the effective isolation of the new design sensor from the mechanical impacts of fluid flowing through the fluid channel, which is a consequence of the rigid adhesion of the sensing element to the polycarbonate base of the fluid chip.

The sensor noise level and its detection limit can be estimated from the standard deviation of the measured dependence at one solution concentration. We calculated the standard deviation for the data presented in Figure 6 from the horizontal line (the abscissa axis) at $1.4 \times 10^{-3} \text{ nm}$. The abscissa axis in this case coincides with the straight line, which is the average value for the presented experimental points. The triple standard deviation, in fact, corresponds to the detection limit of the sensor (LOD).^[26,27] Based on the sensitivity of the sensor of 894 nm RIU^{-1} , the detection limit of the sensor is $4.7 \times 10^{-6} \text{ RIU}$, which is almost half an order of magnitude better than the previously known values obtained with tilted Bragg gratings.^[8,21,24] It should be

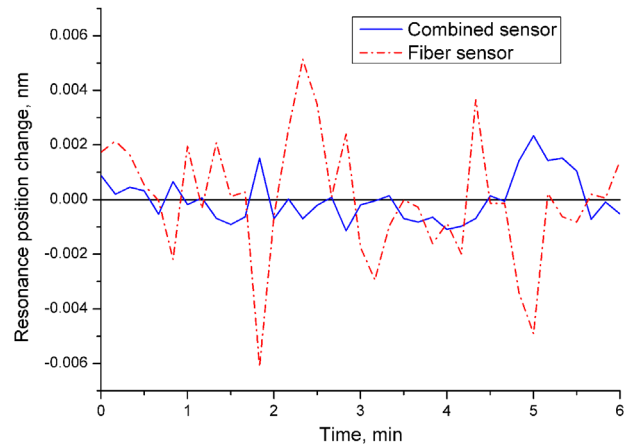


Figure 6. Comparative data on the noise level for a new combined sensor (solid line) and a sensor fixed at two points (dashed line).

noted that, thanks to the developed mathematical apparatus, the data from the sensor are obtained and processed in an automatic mode without the subjective influence of the human factor.

4. Conclusion

A new planar-fiber design of a plasmon sensor based on a TFBG is proposed. Due to the rigid adhesion of the fiber sensor to the base of the microfluidic chip, the sensor is effectively isolated from the possible mechanical influences of the flowing stream, which significantly improves the stability and reproducibility of the sensor's readings. For the spectra processing, an original mathematical apparatus was used. This makes it possible to determine the spectral position of the plasmon resonance from the transmission spectrum of the sensor with high accuracy. The experiments showed a high value of the LOD at the level of $4.7 \times 10^{-6} \text{ RIU}$ and linearity of the sensor in a wide range of refractive indices. The sensitivity of the sensor calculated from the experimental data were approximately 900 nm RIU^{-1} .

Acknowledgement

This work was supported by the Advanced Research Foundation.

Conflict of Interest

The authors declare no conflict of interest.

Keywords

plasmon sensors, refractive index sensors, surface plasmon resonance, tilted fiber Bragg gratings

Received: July 11, 2018
Revised: November 2, 2018
Published online: December 11, 2018

- [1] R. L. Rich, D. G. Myszka, *J. Mol. Recognit.* **2005**, *18*, 431.
- [2] V. Márquez-Cruz, J. Albert, *J. Lightwave Technol.* **2015**, *33*, 3363.
- [3] J. Homola, S. S. Yee, G. Gauglitz, *Sens. Actuators B* **1999**, *54*, 3.
- [4] R. Kashyap, G. Nemova, *J. Sens.* **2009**, *2009*, 645162.
- [5] E. Klantsataya, P. Jia, H. Ebdorff-Heidepriem, T. M. Monro, *Sensors* **2017**, *17*, 12.
- [6] A. Otto, *Z. Phys.* **1968**, *216*, 398.
- [7] E. Kretschmann, H. Raether, *Z. Naturforsch.* **1968**, *23*, 2135.
- [8] C. Caucheteur, T. Guo, J. Albert, *Anal. Bioanal. Chem.* **2015**, *407*, 3883.
- [9] S. K. Srivastava, B. D. Gupta, *Open Opt. J.* **2013**, *7*, 58.
- [10] Y. Zhao, Z. Deng, Q. Wang, *Sens. Actuators B* **2014**, *192*, 229.
- [11] A. Ricciardi, A. Crescitelli, P. Vaiano, G. Quero, M. Consales, M. Pisco, E. Esposito, A. Cusano, *Analyst* **2015**, *140*, 8068.
- [12] K. Tomyshev, D. Tazhetdinova, E. Manuilovich, O. Butov, *J. Appl. Phys.* **2018**, *124*, 113106.
- [13] J. Albert, S. Lepinay, C. Caucheteur, M. C. DeRosa, *Methods* **2013**, *63*, 239.
- [14] C. Ribaut, M. Loyez, J. Larrieu, S. Chevineau, P. Lambert, M. Rimmelink, R. Wattiez, C. Caucheteur, *Biosens. Bioelectron.* **2017**, *92*, 449.
- [15] Y. Shevchenko, J. Albert, *Opt. Lett.* **2007**, *32*, 211.
- [16] Y. Shevchenko, G. Camci-Unal, D. F. Cuttica, M. R. Dokmeci, J. Albert, A. Khademhosseini, *Biosens. Bioelectron.* **2014**, *56*, 359.
- [17] G. Nemova, R. Kashyap, *Opt. Lett.* **2006**, *31*, 2118.
- [18] J. Albert, L. Y. Shao, C. Caucheteur, *Laser Photon. Rev.* **2013**, *7*, 83.
- [19] K. A. Tomyshev, Y. K. Chamorovskiy, V. E. Ustimchik, O. V. Butov, *Proc. SPIE* **2017**, *10323*, 103235K.
- [20] K. A. Tomyshev, D. K. Tazhetdinova, O. V. Butov, *Proc. PIERS* **2017**, *2017*, 53.
- [21] M. Kanso, S. Cuenot, G. Louarn, *Plasmonics* **2008**, *3*, 49.
- [22] C. Ribaut, V. Voisin, V. Malachovská, V. Dubois, P. Mégret, R. Wattiez, C. Caucheteur, *Biosens. Bioelectron.* **2016**, *77*, 315.
- [23] L. Han, T. Guo, C. Xie, P. Xu, J. Lao, X. Zhang, Y. Huang, J. Xu, X. Chen, X. Liang, W. Mao, B. Guan, *J. Lightwave Technol.* **2017**, *35*, 3360.
- [24] V. Voisin, C. Caucheteur, P. Mégret, J. Albert, *Appl. Opt.* **2011**, *50*, 4257.
- [25] K.-Y. Chu, A. R. Thompson, *J. Chem. Eng. Data* **1962**, *7*, 358.
- [26] D. MacDougall, F. J. Amore, G. V. Cox, D. J. Crossby, F. L. Estes, D. H. Freeman, W. E. Gibbs, J. E. Gordon, L. H. Keith, J. Lal, R. R. Langner, N. I. MacClelland, W. F. Phillips, R. B. Pozhasek, R. E. Sievers, R. J. Smerko, D. C. Wimert, W. B. Crummett, R. Libby, H. A. Laitinen, M. M. Reddy, J. K. Taylor, *Anal. Chem.* **1980**, *52*, 2242.
- [27] G. L. Long, J. D. Winefordner, *Anal. Chem.* **1983**, *55*, 712A.